

Performance Of Solar Air Heaters With Corrugated Absorber Plate- A CFD Approach

Dr. Ashwini Kumar

Prof. Avinash Gholap

Prof. Rohit Gangarde

Professor (Asst.), Department of Mechanical Engineering,
H.S.B.P.V.T's GOI, College of Engineering- Parikrama,
Kasthi, India

Shubham M. Shinde

Manoj P. Vyavahare

Vishal B. Mete

Sudhir A. Borude

UG Students Department of mechanical Engineering,
H.S.B.P.V.T's GOI, College of Engineering- Parikrama,
Kasthi, India

Abstract: In recent years CFD has been applied in the design of solar air heater. The studies reported that the quality of the solutions obtained from CFD simulations are largely within the acceptable range proving that CFD is an effective tool for predicting the behavior and performance of a solar air heater. The thermal performance of conventional solar air heater is lower as compared to that of corrugated absorber plate solar air heaters. There are various types of corrugation like W-shape, V-shape; sine wave shape etc. can be used as absorber plate. The use of corrugation in different forms and shapes is an effective and economic way of improving the performance of solar air heaters. Use of corrugated absorber plate in solar air heater duct increases the Nusselt number and the friction factor with the increase in mass flow rates, the Nusselt number increases and the friction factor decreases for all combination of mass flow rates. In the present investigation the effect of flow parameters on flow field, temperature field and heat transfer has been analyzed. Also the comparison of the result obtained by the present CFD analysis with previous experimental results has been shown.

Keywords: CFD Analysis; Absorber plate; Solar air heaters; Nusselt number; Reynolds number.

NOMENCLATURE

D_h	hydraulic diameter of duct, mm	f_s	friction factor of smooth absorber plate
P_h	wetted perimeter, mm	N_{uc}	Nusselt number
A	cross-sectional area, m^2	N_{uc}	Nusselt number of corrugated absorber plate
h	heat transfer coefficient, W/m^2K	N_{us}	Nusselt number of smooth absorber plate
k	thermal conductivity of air, W/mK	Pr	Prandtl number
$L1$	inlet length of duct, mm	Re	Reynolds number
$L2$	test length of duct, mm	W/H	Duct aspect ratio
$L3$	outlet length of duct, mm	δ	Transition sub-layer thickness, mm
H	depth of duct, mm	μ	Dynamic viscosity, Ns/m^2
W	width of duct, mm	ρ	Density of air, kg/m^3
m	mass flow rate, kg/s	τ	Wall shear stress, Kg/m^2
ΔP	pressure drop, Pa		
f	friction factor		
f_c	friction factor of corrugated absorber plate		

I. INTRODUCTION AND LITERATURE SURVEY

In present world the prosperity of nation is measured by the energy consumption of that nation, the GDP of country is directly linked with energy consumption. Therefore demand for energy resources is increasing day by day. There are various types of energy resources but mainly they are classified in commercial and non-commercial energy, renewable and non-renewable energy and primary and secondary energy forms. From renewable point of view solar energy is one of the most convenient forms. It is the energy which is coming from sun in the form of light and heat. Especially the thermal energy will be further converted into electrical energy. One of the most potential applications of solar energy is the supply of hot air for drying of agricultural and heating of buildings to maintain a comfortable environment especially in the winter season. The large magnitude of solar energy available makes it a highly appealing source of electricity.

Solar air heater is one of the basic equipment through which solar energy is converted into thermal energy. A conventional solar air heater generally consist of an absorber plate, a rear plate, insulation below the rear plate, transparent cover on the exposed side, and the air flows between the absorbing plate and rear plate. The value of the heat transfer coefficient between the absorber plate and air is low and this result in lower efficiency for this reason the surface are sometime roughened in the air flow passage. Fig. 1 shows a conventional solar air heater. There are basically three approaches or methods that can be used to solve a problem of fluid flow and heat transfer. These approaches are: Experimental, Theoretical and Computational (CFD).

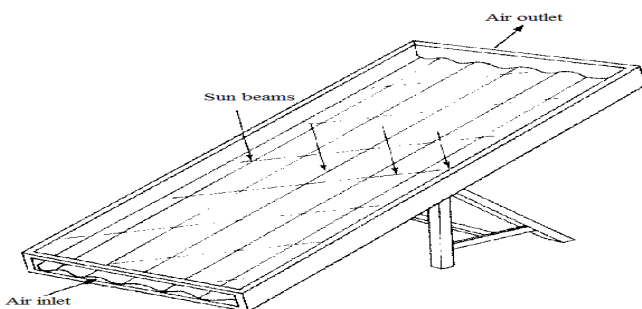


Figure 1: Conventional solar air heater

The most reliable information about a physical process is often given by actual measurement. An experimental approach involving full-scale equipment can be used to predict how identical copies of the equipment would perform under the same conditions. Such full scale tests are, in most cases, prohibitively expensive and often impossible. The alternative then is to perform experiments on small-scale models. The resulting information however must be extrapolated to full scale, and general rules for doing this are often unavailable. Further, the small-scale models do not always simulate all the features of the full-scale equipment; frequently, important features such as combustion or boiling are omitted from the model tests. This further reduces the usefulness of the test results. Finally it must be remembered that there are serious difficulties of measurement in many situations, and that the measuring instruments are not free from errors.

A theoretical prediction works out the consequences of a mathematical model, rather than those of an actual physical model. For the physical processes of interest, the mathematical model mainly consists of a set of differential equations. If the methods of classical mathematics were to be used for solving these equations, there would be little hope of predicting many phenomena of practical interest. In the theoretical approach simplifying assumptions are used in order to make the problems tractable.

Computational fluid dynamics or CFD is the analysis of systems involving fluid flow, heat transfer and associated phenomena such as chemical reactions by means of computer-based simulation. The technique is very powerful and spans a wide range of industrial and non-industrial application areas. The equations governing the fluid flow are the continuity (conservation of mass), the Navier–Stokes (balance of momentum), and the energy (conservation of energy) equations. These equations form a system of coupled non-linear partial differential equations (PDEs). Because of the coupled nature of the equations and the presence of non-linear terms, the fluid flow equations are generally not amenable to analytical method of obtaining the solution. In general, closed form analytical solutions are possible only if these PDEs can be made linear, either because non-linear terms naturally drop out (as in the case of parallel flows or flows that are in viscous and irrotational everywhere) or because the nonlinear terms are small compared to other terms so that they can be neglected (e.g., creeping flows, small amplitude sloshing of liquid etc.). If the non-linearities in the governing PDEs cannot be neglected, which is often the case for most engineering flows, one normally has to resort to numerical methods to obtain solutions.

Many researchers worked on solar air heater to enhance thermo-hydraulic performance. Bhagoria et al. [1] performed experiments to find out the effect of relative roughness pitch and height respectively on the heat transfer and friction factor in a solar air heater with wedge shaped rib roughness and found maximum enhancement of Nusselt number is up to 2.4 times whereas the friction factor increased by 5.3 times for the investigated range of parameters. Karim and Hawladar [2] and Karim et al. [3] experimentally found that the v-corrugated collector has superior thermal performance compare to flat plate collector. Lin et al. [4] found that cross-corrugated solar air-heaters have a better thermal performance than the flat-plate collector. Saini and Saini [5] from their performed experiments found 3.8 times enhancement in Nusselt number and 1.75 times enhancement in friction factor in duct having transverse ribs. Vishavjeet et al. [6] discussed that CFD analysis is now very important for the study of flow behavior and various performance characteristics of solar air heater and it will be carried out to find optimum roughness parameters. Hüseyin Benli [7] experimentally found that the corrugated collectors have much higher thermal performance as compared to flat plate collectors because of more surface area for absorption of heat. K. Vasudeva Karanth [8] found that absorber plate with corrugated geometry helps to enhance the Nusselt number which in turn helps in increased convective heat transfer. Yadav and Bhagoria [9] performed a numerical analysis of heat transfer and fluid flow characteristics in an artificially roughened solar air heater and found maximum

value of the thermo-hydraulic performance is 1.82. Prasad [10] experimentally investigated the effects of artificial roughness on heat transfer and friction factor characteristics of solar air heaters. The maximum value of the ratio of collector heat removal factor is 1.786, collector efficiency factor is 1.806 and thermal efficiency is 1.842 times more compared to smooth absorber plate solar air heaters. However the extension of this work has been worked out by Prasad et al. [11] for three sides wire mesh artificial roughness, which was further optimized by Prasad et al. [12] and investigated [13-15]. Prasad et al. [11] experimentally conduct an analysis for the fluid flow and heat transfer behaviour in a solar air heater with artificial roughness of very small diameter wires on the three sides (one at top side and other at two side walls) of the rectangular duct solar air heater. Authors have found that the values of Nusselt number friction losses for three sides artificially roughened solar air heater are (20-75%) and (2-34%) more as compared to the only one side roughened one. In this path of heat transfer analysis Kumar et al. [16], have shown the effects of glass covers on net heat transfer rate and found that rate of heat transfer rate increases with the increasing sides of glass covers. Hawang and Liou [17] investigated the heat transfer on a channel having perforated fences. Author compared the thermal performance of three different types of turbulence promoters perforated solid and slit types and found that perforations in turbulence promoters increase the heat transfer. Buchlin [18] investigated the heat transfer in a channel with various types of perforated rib and found enhanced heat transfer as compare to smooth channel. Shaeri and Yaghoubi [19] numerically studied the effect of perforated fin on pressure drop and heat transfer. The use of booster mirrors for three sides artificially roughened solar air heaters for the enhancement of collector performance has been shown [20-21]. A brief review report on collector performance has been given by Kumar and Alam [22]. But most of the analysis on solar air heater duct and rib roughness has been conducted experimentally and very few studies have been reported using the computational fluid dynamics (CFD) [23-28]. The present paper has been prepared to study the effect of flow parameters on flow field, temperature field and heat transfer and to compare the result obtained by the present CFD analysis with previous experimental results.

II. MATHEMATICAL MODELLING

The model designed and simulated for study of various flow parameters in solar air heater is in accordance with the ASHRAE 93-2003 as shown in Fig. 2. According to these standard whole flow field is divided into three sections i.e. the entry section, the test section and the exit section. The first section is the entry section and is provided so that the flow is fully developed before entering into test section. The corrugated absorber plate to be investigated is used in the test section. The exit section is provided to make sure that the effect of flow at exit is not affecting the test section. The model developed for the current study is as shown below.

ABSORBER PLATE

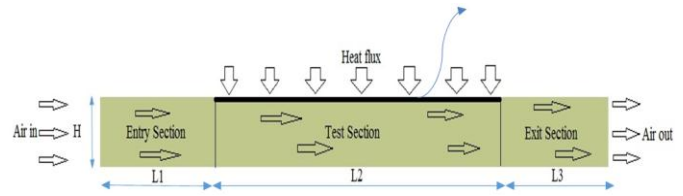


Figure 2: Computational domain of solar air heater

A. GOVERNING EQUATIONS

The forced turbulent fluid flow and heat transfer in the artificially roughened solar air heater are described by the governing equations of flow continuity, and conservation of momentum and energy. With assumptions of 2-dimensional steady state, forced turbulent flow, incompressible fluid, and no radiation heat transfer, the governing equations in the rectangular Cartesian coordinate system are as follows:

The Continuity equation is:

$$\frac{\partial}{\partial x_i} (\rho u_i) = 0 \quad (1)$$

Where ρ is the density of fluid and u_i is the axial velocity.

The Momentum equation is:

$$\frac{\partial}{\partial x_j} (\rho u_i u_j) = -\frac{\partial p}{\partial x_i} + \frac{\partial}{\partial x_j} \left[\mu \left(\frac{\partial u_i}{\partial x_j} + \frac{\partial u_j}{\partial x_i} \right) \right] + \frac{\partial}{\partial x_j} (-\rho \overline{u_i u_j}) \quad (2)$$

Where μ , \overline{u} , and u_j , are the fluid viscosity, fluctuated velocity, and the axial velocity, respectively, and the term $\rho \overline{u_i u_j}$ is the turbulent shear stress. The Reynolds-averaged approach to turbulence modelling requires that the Reynolds stresses $-\rho \overline{u_i u_j}$ in Eq. (2) needs to be modelled. For closure of the equations, the k- ϵ turbulence model is chosen. A common method employs the Boussinesq hypothesis to relate the Reynolds stresses to the mean velocity gradients:

$$-\rho \overline{u_i u_j} = \mu_t \left(\frac{\partial u_i}{\partial x_j} + \frac{\partial u_j}{\partial x_i} \right) \quad (3)$$

The Energy equation is:

$$\frac{\partial}{\partial x_i} (\rho u_i T) = \frac{\partial}{\partial x_j} \left[(\Gamma + \Gamma_t) \frac{\partial T}{\partial x_j} \right] \quad (4)$$

Where Γ and Γ_t are molecular thermal diffusivity and turbulent thermal diffusivity, respectively and are given by

$$\Gamma = \frac{\mu}{Pr} \quad , \quad \text{and} \quad \Gamma_t = \frac{\mu}{Pr_t} \quad (5)$$

The turbulent viscosity term μ_t is to be computed from an appropriate turbulence model. The expression for the turbulent viscosity is given as

$$\mu_t = \rho C_\mu \frac{k^2}{\epsilon} \quad (6)$$

There are two additional equations for the k-epsilon turbulent model:

Turbulent kinetic energy (k)-

$$\frac{\partial}{\partial x_j} (\rho k u_i) = \frac{\partial}{\partial x_j} \left[\left(\mu + \frac{\mu_t}{\sigma_k} \right) \frac{\partial k}{\partial x_j} \right] + G_k - \rho \epsilon \quad (7)$$

Rate of dissipation (ϵ)-

$$\frac{\partial}{\partial x_i} (\rho \epsilon u_i) = \frac{\partial}{\partial x_j} \left[\left(\mu + \frac{\mu_t}{\sigma_\epsilon} \right) \frac{\partial \epsilon}{\partial x_j} \right] + C_{1\epsilon} \frac{\epsilon}{k} G_k - C_{2\epsilon} \rho \frac{\epsilon^2}{k} \quad (8)$$

In the above equation, G_k represents the rate of generation of the turbulent kinetic energy due to mean velocity gradients while $\rho\varepsilon$ is its destruction rate. The σ_k and σ_ε are effective Prandtl numbers for turbulent kinetic energy and rate of dissipation, respectively; $C_{1\varepsilon}$ and $C_{2\varepsilon}$ are constants. G_k is written as:

$$G_k = -\rho \overline{\dot{u}_i \dot{u}_j} \frac{\partial u_i}{\partial x_j} \quad (9)$$

The boundary values for the turbulent quantities near the wall are specified with the enhanced wall treatment method. $C_\mu=0.09$, $C_{1\varepsilon}=1.44$, $C_{2\varepsilon}=1.92$, $\sigma_k=1.0$, $\sigma_\varepsilon=1.3$ and $Pr_t=0.9$ are chosen to be empirical constants in the turbulence transport equations. The governing equations are solved using a finite volume approach and the SIMPLE algorithm. The solutions are considered to be converged when the normalized residual values reach 10^{-5} for all variables.

B. BOUNDARY CONDITIONS

The solution domain consist of a duct on the x–y plane, enclosed by the inlet, outlet and wall boundaries. Since the Navier-Stokes equations are solved inside the computational domain, no-slip boundary conditions are applied on the duct walls for all cases. The tangential component of fluid velocity equals that of the solid at the interface represents no-slip boundary condition. The bottom surface is adiabatic i.e. insulated, and a constant heat flux (910 W/m^2) is applied on the top surface of the solar air heater. The temperature of air inside the duct is also taken as 300 K at the beginning. At the inlet of the computational domain, the mass flow rate inlet boundary condition is specified. Mass flow rate inlet boundary conditions are commonly used to define the flow velocity, along with all relevant scalar properties of the flow, at flow inlets. A uniform air mass flow rate is introduced at the inlet. In this simulation, eleven uniform mass flow rates and a fixed air temperature of 300 K are appointed at the domain inlet. The mean inlet velocity of the flow is calculated using Reynolds number. The outflow boundary condition is appointed at the exit of the computational domain. A pressure outlet boundary condition is applied with a fixed pressure of $1.013 \times 10^5 \text{ Pa}$ at the exit.

C. PROPERTIES OF MATERIALS USED

Here two types of materials are used which is air and aluminium. Air is acting as a working fluid and aluminium sheet is used as absorber plate material. The various properties of these two materials are given below in tabular form.

Surface	Boundary condition	Value
Inlet	Mass flow inlet	(0.05 - 0.15) kg/s
Outlet	Pressure outlet	0 Pascal (gauge)
Top surface	Wall	Heat flux = 910 W/m^2
Bottom surface	Wall	Adiabatic wall

Table 1: Boundary condition of study domain

Properties	Air	Aluminium
Density(kg/m^3)	1.225	2719
Specific heat(J/kg-K)	1006	871
Thermal	0.0242	202.4

conductivity(W/m-K)		
Viscosity(N s/m^2)	1.7894×10^{-5}	-

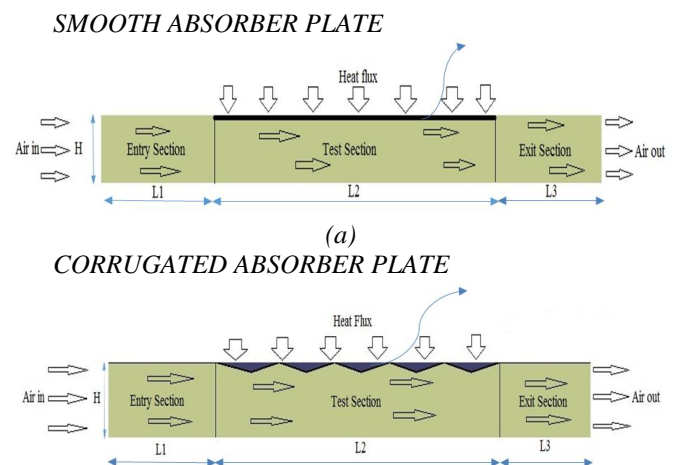
Table 2: Properties of materials used in computational domain

III. CFD INVESTIGATION

The commercial finite-volume based CFD code ANSYS FLUENT v 14.5 has been used to simulate fluid dynamics and heat transfer and also to solve the conservation equations for mass, momentum and energy. Computational domain, grid generation, selection/validation of appropriate turbulence model and solution procedure is presented in detail in the following sub-sections.

A. COMPUTATIONAL DOMAIN

The computational model is designed and simulated for study of various flow parameters in solar air heater is in accordance with the ASHRAE 93-2003. According to these standard whole flow field is divided into three sections i.e. the entry section, the test section and the exit section as shown in Fig. 3(a) &(b). The first section is the entry section (entry section must be equal to or greater than $5\sqrt{WH}$) and is provided so that the flow is fully developed before entering into test section, length of the entry section is taken as 500mm. The corrugated surface to be investigated is used in the test section. The test section consists of an absorber plate which has a length of 1200 mm and width of 300 mm, the thickness of the plate is taken to be 0.8 mm. The air domain is provided with 30mm height with same length and width as in absorber plate. The exit section (exit section must be equal to or greater than $2.5\sqrt{WH}$) is provided to make sure that the effect of flow at exit is not affecting the test section; length of exit section is taken as 450mm. Here two ducts are taken one is containing smooth absorber plate as shown in Fig. 3 (a) and other is corrugated absorber plate as shown in Fig. 3 (b). Various assumptions taken are: flow is steady and two dimensional, air is compressible, the physical and thermal properties of the absorber plate is taken as constant with respect to the operating temperature, constant value of heat flux is taken over the absorber plate as solar insolation.



(b)

Figure 3: Computational domain for (a) smooth solar air heater (b) corrugated absorber plate solar air heater

The duct wall and absorber plate material are homogeneous and isotropic. Fig. 4 shows the basic W shaped corrugated geometry of absorber plate. Corrugations are having a total depth of 3 mm towards the absorber air chamber. The corrugations are provided equally at an axial distance of 50mm, all along the flow length of absorber duct.

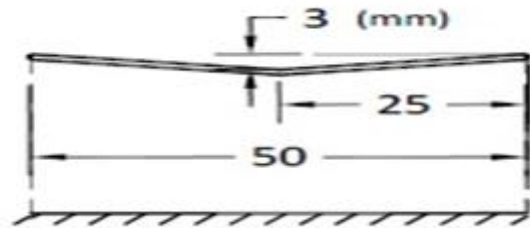


Figure 4: Corrugated geometry of absorber plate

B. GRID GENERATION

One of the most important tasks in developing the 2D CFD simulation is to generate adequate fine grid to ensure accurate flow computations. Uniform grids are generated for all numerical simulations performed in this work. Uniform grids are commonly used in modeling when large gradients are expected. An exponential function is used to concentrate the fine mesh near the wall to resolve the high-velocity gradients near the walls. Grids are generated using ANSYS ICEM CFD v14.5 software. A uniform grid contained 173383 quad nodes and 170058 elements with cell size of 0.0001m is used to resolve the laminar sub-layer, as shown in Fig. 5.

Entrance length of duct (L1)	500mm
Test length of duct (L2)	1200mm
Exit length of duct (L3)	450mm
Width of duct (W)	300mm
Depth of duct (H)	30mm
Duct aspect ratio (W/H)	10
Uniform heat flux (I)	910W/m ²
Mass flow rate (m)	(0.005 – 0.015)kg/s
Reynolds number (R_g)	4475 - 13410
Prandtl number (Pr)	0.7441

Table 3: Geometrical and operating parameters for computational analysis

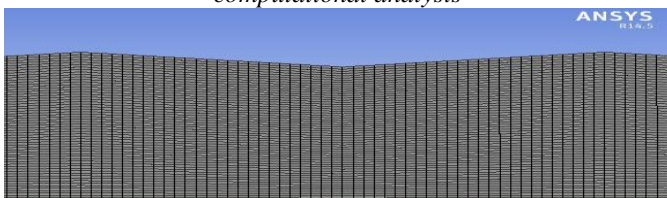


Figure 5: 2D closed mesh view

An extensive test for the confirmation of grid independence of the model are carried out by increasing the mesh density and adopting various mesh grading until further refinement shows a difference of less than 1% in two consecutive sets of results. Fig. 5 shows the two dimensional closed mesh view of the corrugated absorber plate.

C. SELECTION OF APPROPRIATE TURBULENCE MODEL

To achieve the accurate prediction of heat transfer and friction factor in a solar air heater, the predictive ability of five different turbulence models including: The Standard k-epsilon turbulence model, the Realizable k-epsilon turbulence model, the Renormalization-group (RNG) k-epsilon turbulence model, the Standard k-omega turbulence model, and the Shear Stress Transport (SST) k-omega turbulence model, are investigated. The smooth duct having same cross section was compared with Dittus-Boelter empirical correlation for Nusselt number and Blasius equation for Friction factor.

$$\text{Dittus-Boelter equation: } N_u = 0.023 R_g^{0.8} Pr^{0.4} \quad (9)$$

$$\text{Blasius equation: } f = 0.079 R_g^{-0.25} \quad (10)$$

To analyze and compare the flow characteristics and heat transfer following parameters is used:-

Hydraulic diameter (D_h)

$$D_h = \frac{4A}{P_h} \quad (11)$$

Where A is cross-section area and P_h is wetted perimeter of the cross section.

The relevant non-dimensional parameters of interest in the present CFD investigation are the Reynolds number, Nusselt number and friction factor.

Reynolds number is defined as

$$R_g = \frac{\rho v D_h}{\mu} \quad (12)$$

Nusselt number is defined as

$$N_u = \frac{h D_h}{k} \quad (13)$$

Pressure drop is calculated using the following correlation:

$$\Delta P = \frac{2f \rho l v^2}{D_h} \quad (14)$$

Fig. 8 to Fig. 12 and Fig. 13 to Fig. 17 shows the variation of Nusselt number and friction factor with Reynolds number for different turbulence models respectively, The empirical correlation available for conventional solar air heater i.e., Dittus-Boelter equation and Blasius equation. For different models and the results are compared with results computed from Dittus-Boelter empirical relationship for a smooth duct. It has been observed that the results obtained by Renormalization-group (RNG) k-epsilon model are in good agreement with Dittus-Boelter equation and Blasius equation empirical results. Results obtained by Realizable k-epsilon model have less deviation with empirical correlation results; whereas results obtained by other models namely Standard k-epsilon, Standard k-omega and SST k-omega have more deviation.

D. SOLUTION PROCEDURE

In the present simulation governing equations of continuity, momentum and energy are solved by the finite volume method in the steady-state regime using the commercial CFD code ANSYS FLUENT v14.5. A second-order upwind scheme is chosen for both energy and momentum equations. Double precision pressure based solver

is selected in order to solve the set of equations used. Second order upwind discretization scheme is selected for all the transport equations. Whenever convergence problems are noticed, the solution is started using the first order upwind discretization scheme and continued with the second order upwind scheme. The governing equations for mass and momentum conservation are solved with a segregated approach in steady state, where equations are sequentially solved with implicit linearization. The SIMPLE algorithm (semi-implicit method for pressure linked equations) is chosen as scheme to couple pressure and velocity. The convergence criteria of 10^{-6} for the residuals of the continuity equation, 10^{-6} for the residuals of the momentum equation, 10^{-3} for the residuals of the velocity components and 10^{-6} for the residuals of the energy are assumed. The heat transfer coefficient at the solid fluid interface was also monitored to assure the convergence of the solution.

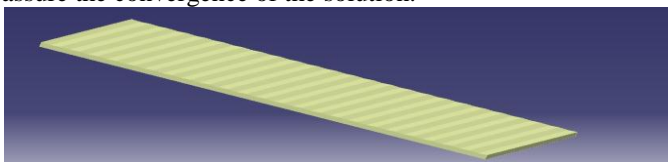


Figure 6: 3D view of duct with corrugated absorber plate

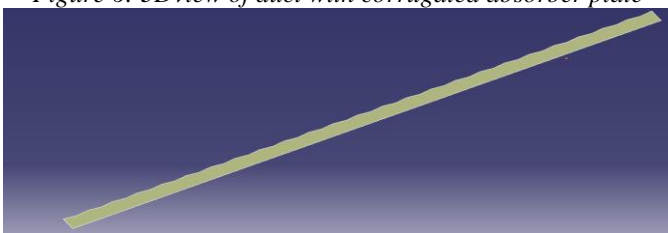


Figure 7: 2D view of duct with corrugated absorber plate

IV. RESULTS AND DISCUSSION

CFD computations of heat transfer and fluid flow characteristics in solar air heater with corrugated absorber plate are performed. The effects of grid density, Reynolds number, and corrugated surface on the average heat transfer for flow of air in solar air heater are discussed below. In order to validate the CFD data, comparison of Nusselt number and friction factor for smooth duct under present CFD investigation (generated by the correlations) are plotted and compared as shown in Fig. 8 to Fig. 12 and Fig. 13 to Fig. 17 respectively. Also comparison of Nusselt number and friction factor for smooth duct and duct with corrugated absorber plate are plotted as shown in Fig. 18 and Fig. 19 respectively. Various contours (pressure, static temperature, turbulence kinetic energy and velocity) generated using CFD post processors are shown in Fig. 21 to Fig. 32.

A. GRID INDEPENDENCE TEST

To study the variation of heat transfer and flow characteristics with change in grid size, grid independence study is carried out. Seven sets of grids with different sizes are used for the simulation to assure that the results are grid independent. Grid independence test is carried out over grids with different numbers of nodes in seven steps. It is found that the variation in Nusselt number slightly increases (up to \pm

0.25%) when moving from 173383 nodes to 196472. Hence, there is no such advantage in increasing the number of nodes beyond this value. Thus, the grid system of 173383 nodes is adopted for the present computation.

No of nodes	No of elements	Nusselt no.(CFD)	% Difference Nusselt no.
70468	67502	39.3231	----
90781	87952	40.1452	1.99
115305	112209	40.6451	1.87
131100	127985	41.3743	1.67
151519	148480	41.9510	0.99
173383	170058	42.5112	0.74
196472	192895	42.6110	0.25

Table 4: Grid Sensitivity Test

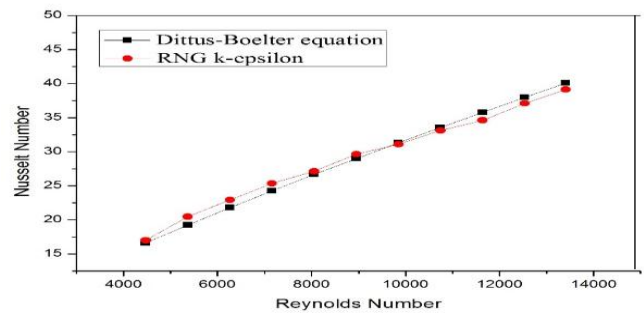


Figure 8: Variation of Nusselt number with Reynolds number using RNG k-epsilon turbulence model

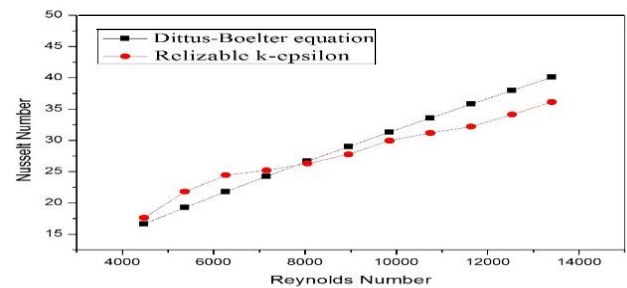


Figure 9: Variation of Nusselt number with Reynolds number using Realizable k-epsilon turbulence model

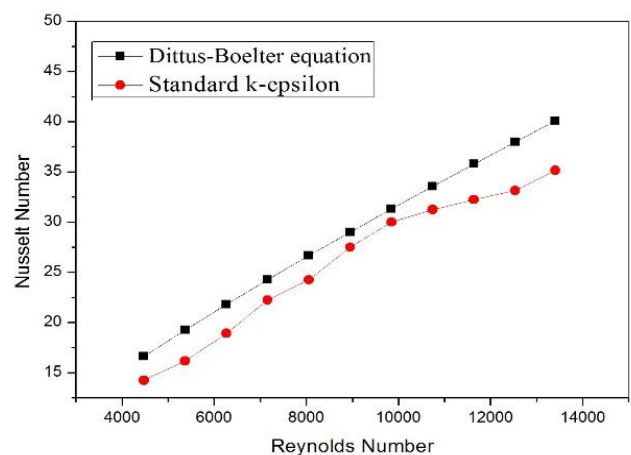


Figure 10: Variation of Nusselt number with Reynolds number using Standard k-epsilon turbulence model

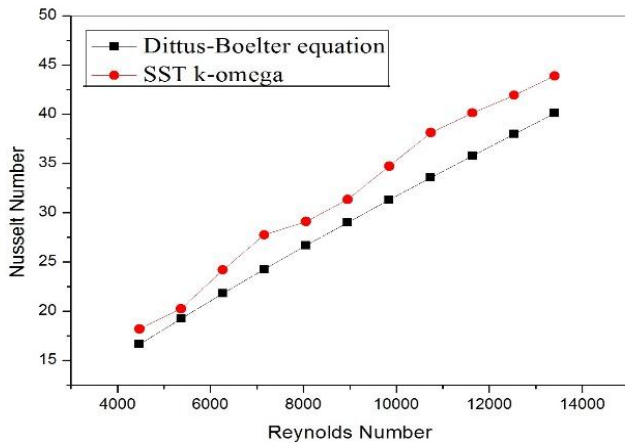


Figure 11: Variation of Nusselt number with Reynolds number using SST k-omega turbulence model

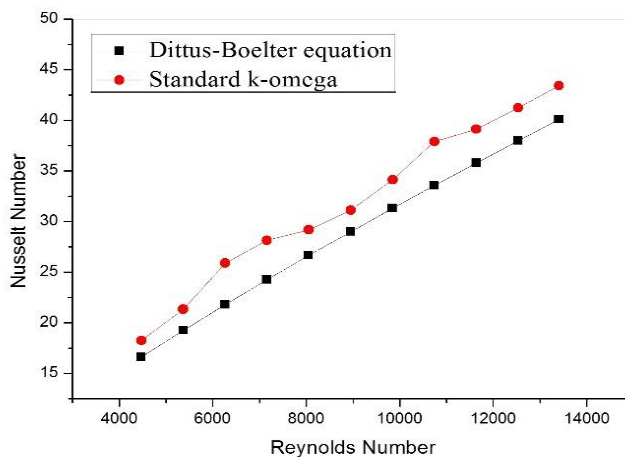


Figure 12: Variation of Nusselt number with Reynolds number using Standard k-omega turbulence model

From Fig. 8 to Fig. 12 it is observed that the results obtained by Renormalization-group (RNG) k-epsilon model are in good agreement with the Dittus-Boelter empirical correlation results. The average absolute percentage deviations between the values predicted by Realizable k-epsilon model and Dittus-Boelter empirical correlation results is found to be $\pm 3\%$ for average Nusselt number. Prediction by Standard k-epsilon, Standard k-omega and SST k-omega model shows more deviation with Dittus-Boelter empirical correlation results.

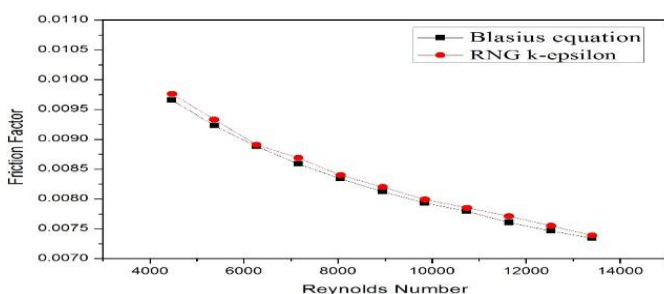


Figure 13: Variation of Friction Factor with Reynolds number using RNG k-epsilon turbulence model

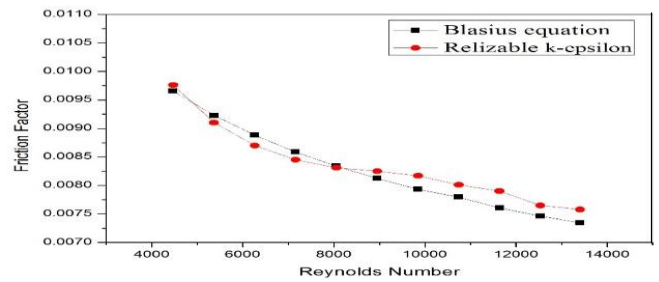


Figure 14: Variation of Friction Factor with Reynolds number using Realizable k-epsilon turbulence model

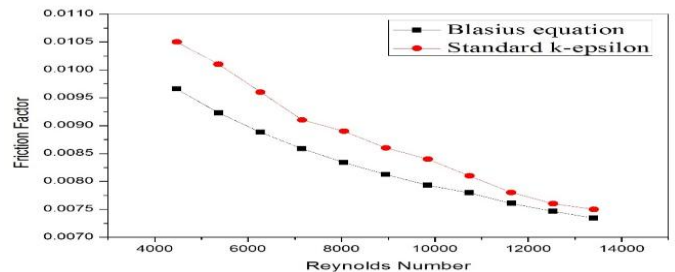


Figure 15: Variation of Friction Factor with Reynolds number using Standard k-epsilon turbulence model

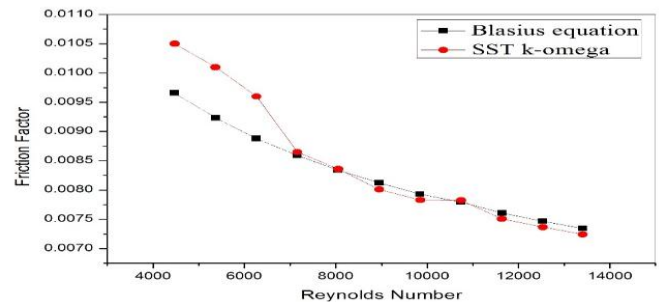


Figure 16: Variation of Friction Factor with Reynolds number using SST k-omega turbulence model

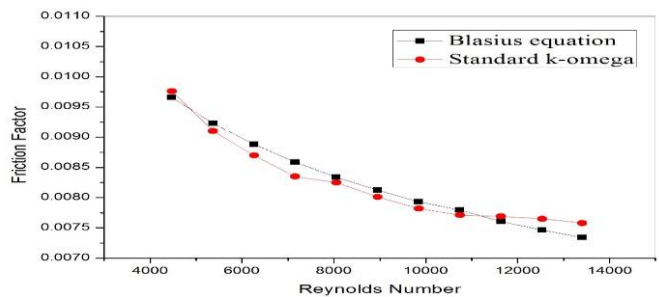


Figure 17: Variation of Friction Factor with Reynolds number using Standard k-omega turbulence model

From Fig. 13 to Fig. 17 it is also observed that the results obtained by Renormalization-group (RNG) k-epsilon model are in good agreement with the Blasius equation empirical correlation results. The average absolute percentage deviation between the values predicted by Standard k-omega model and Blasius empirical correlation results is found to be $\pm 2.5\%$ for average friction factor. Prediction by Standard k-epsilon, Realizable k-epsilon and SST k-omega model Shows more deviation with Blasius empirical correlation results. Five different turbulence models, for steady state conditions, available in FLUENT, are tested and the Renormalization-group (RNG) k-epsilon model is proven as the most appropriate because it can be easily observed that the Renormalization-group (RNG) k-epsilon turbulence model

predicts very close results. This yields confidence in the predictions done by CFD analysis in the design of a solar air heater.

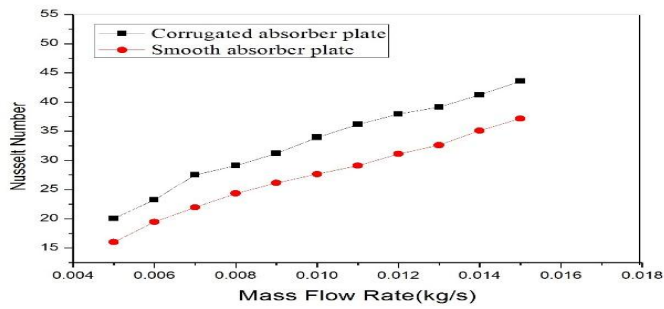


Figure 18: Variation of Nusselt number with mass flow rate for smooth and corrugated absorber plate

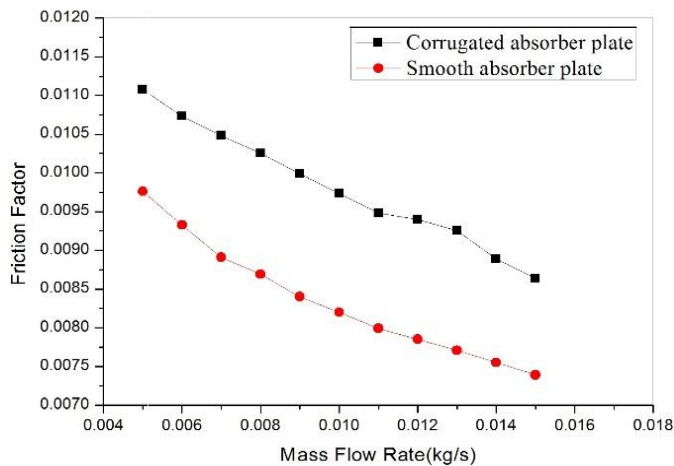


Figure 19: Variation of Friction factor with mass flow rate for smooth and corrugated absorber plate

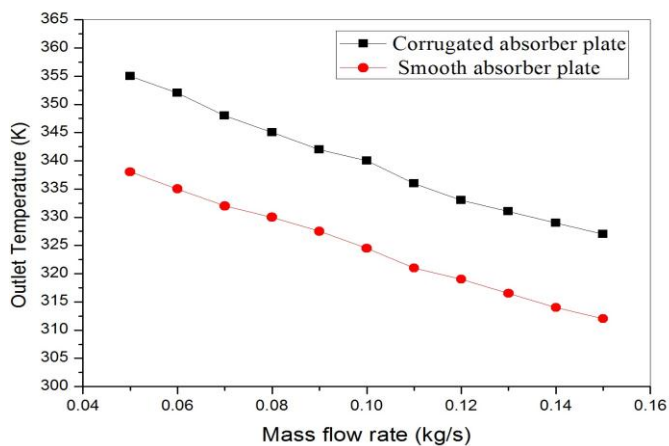


Figure 20: Variation of Outlet temperature with mass flow rate for smooth and corrugated absorber plate

Fig. 18 shows the value of Nusselt number increases with increasing mass flow rate for both smooth and corrugated absorber plate. But it is observed that value of Nusselt number is more in corrugated absorber plate as compared to smooth absorber plate. Fig. 19 shows Friction factor decreases with increasing mass flow rate for both smooth and corrugated absorber plate. Fig. 20 shows the Variation of Outlet temperature with mass flow rate for smooth and corrugated absorber plate, Temperature decreases with increasing mass flow rate.

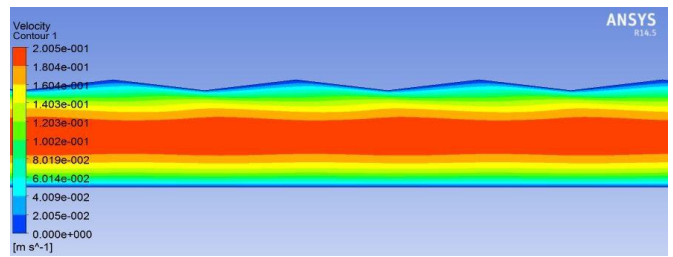


Figure 21: The contour plot of velocity for mass flow rate of 0.005kg/s

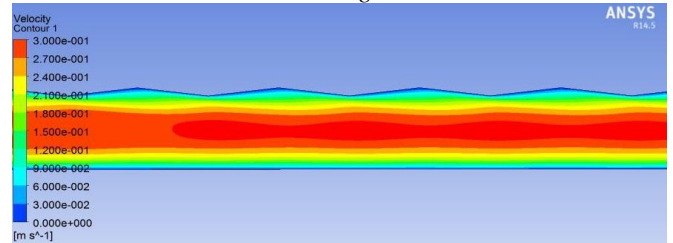


Figure 22: The contour plot of velocity for mass flow rate of 0.010kg/s

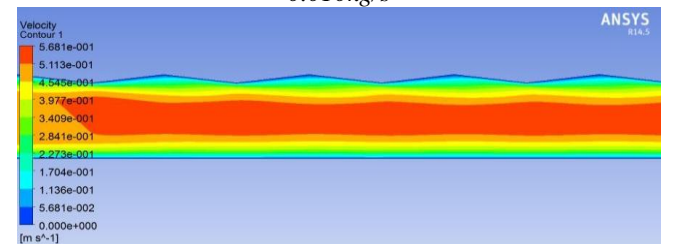


Figure 23: The contour plot of velocity for mass flow rate of 0.015kg/s

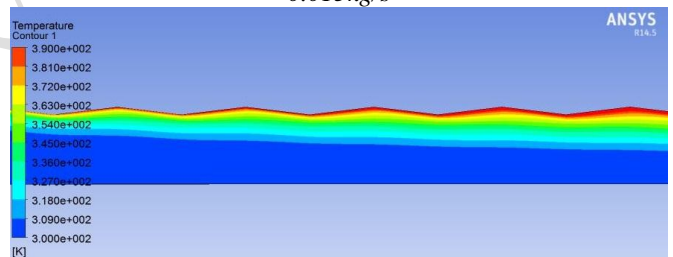


Figure 24: The contour plot of static temperature for mass flow rate of 0.005kg/s

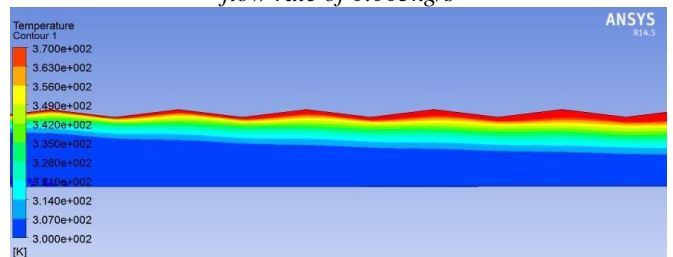


Figure 25: The contour plot of static temperature for mass flow rate of 0.010kg/s

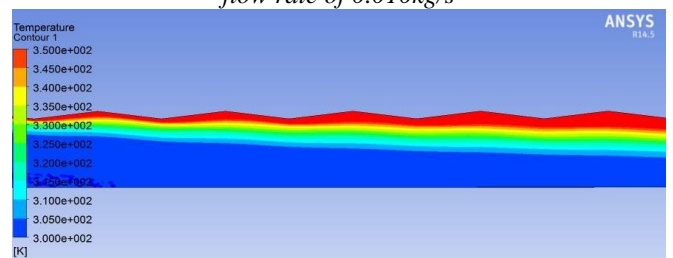


Figure 26: The contour plot of static temperature for mass flow rate of 0.015kg/s

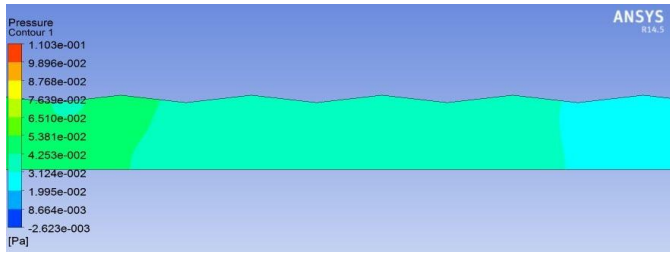


Figure 27: The contour plot of pressure for mass flow rate of 0.005kg/s

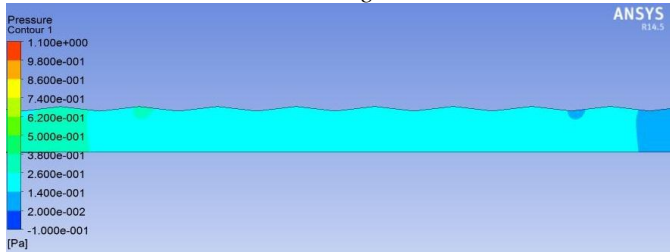


Figure 28: The contour plot of pressure for mass flow rate of 0.010kg/s

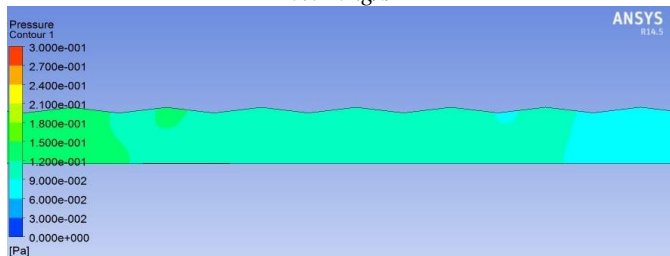


Figure 29: The contour plot of pressure for mass flow rate of 0.015kg/s

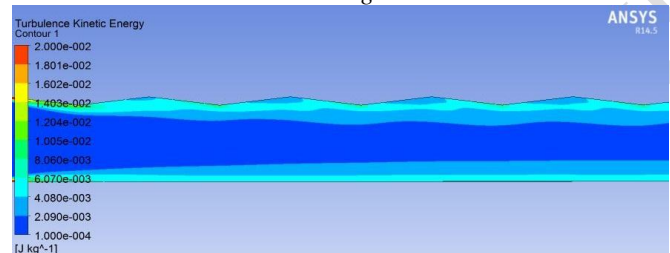


Figure 30: The contour plot of turbulence kinetic energy for mass flow rate of 0.005kg/s

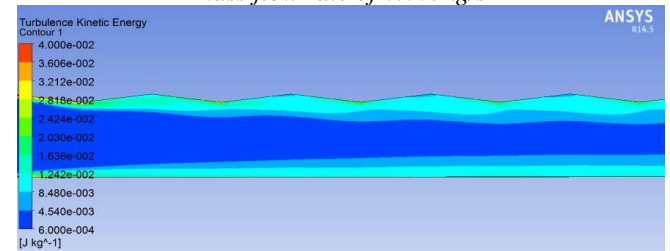


Figure 31: The contour plot of turbulence kinetic energy for mass flow rate of 0.010kg/s

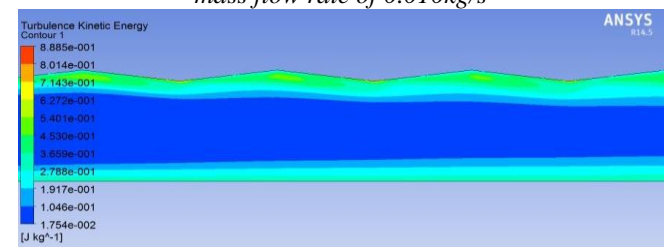


Figure 32: The contour plot of turbulence kinetic energy for mass flow rate of 0.015kg/s

Fig. 21 to Fig. 23 shows the velocity contour for various mass flow rates. The velocity of air near the wall boundary is less and it increases with increasing distance from the two adjacent walls. Fig. 24 to Fig. 26 shows the static temperature contour, as the insolation (heat flux) is applied on the upper side wall i.e. absorber plate so the temperature of the upper side is very high and the temperature decreases in the direction of the lower wall due to insulation. Fig. 27 to Fig. 29 shows the pressure contour, the pressure is gradually decreases to the outlet direction. Fig. 30 to Fig. 32 show the contour of turbulence kinetic energy, which increases in wall. It can be seen that as the mass flow rate increases the static temperature of the flow field decreases. It can also be observed that diffusion of temperature into the core of flow field decreases as the mass flow rate increases but near the wall diffusion of temperature increases as mass flow rate increases.

Mass flow rate (m) in kg/s	Outlet temperature (To) in K	Nusselt no. (Nu)	Friction factor (f)
0.005	355	20.05	0.01108
0.006	352.5	23.25	0.01073
0.007	350.1	26.51	0.01048
0.008	348.1	28.1	0.01025
0.009	345.1	30.21	0.00999
0.010	342.1	32.95	0.00973
0.011	339.1	34.15	0.00948
0.012	336.1	36.95	0.0094
0.013	333.1	38.15	0.00925
0.014	330.1	40.25	0.00889
0.015	327.4	42.51	0.00864

Table 5: Result obtained by CFD for corrugated absorber plate

Table 4 shows the values of Nusselt number enhancement ratio, friction factor enhancement ratio and thermo- hydraulic performance.

Mass flow rate(kg/s)	(N _{uc} /N _{us})	(f _c / f _s)	(N _{uc} /N _{us}) / (f _c / f _s) ^{1/3}
0.005	1.1912	1.8675	0.9665
0.006	1.2123	1.8602	0.9840
0.007	1.2645	1.8468	1.0271
0.008	1.2832	1.8401	1.0447
0.009	1.3178	1.8374	1.0697
0.01	1.3495	1.8182	1.0980
0.011	1.3846	1.8035	1.1339
0.012	1.4198	1.7699	1.1658
0.013	1.4411	1.7496	1.1952
0.014	1.4314	1.6931	1.2000
0.015	1.4616	1.6545	1.2357

Table 6: Thermo- hydraulic performance

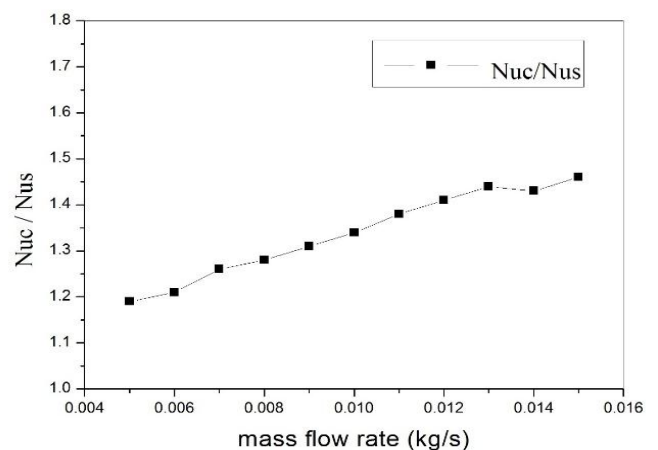


Figure 33: Variation of Nusselt number enhancement ratio with mass flow rate

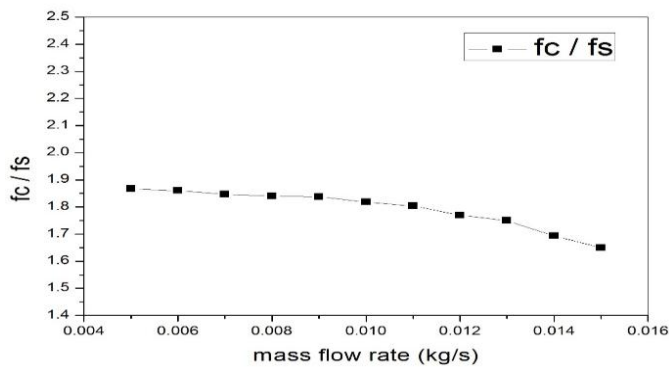


Figure 34: Variation of Friction factor enhancement ratio with mass flow rate

Fig. 33 shows the Variation of Nusselt number enhancement ratio with mass flow rate. Maximum Nusselt number enhancement ratio is 1.4616. Fig. 34 shows Friction factor enhancement ratio with mass flow rate. Maximum Friction factor enhancement ratio is 1.8675. Maximum thermo- hydraulic performance is 1.2357

A. VALIDATION OF THE PRESENT RESULT

In order to validate the present numerical model, the results are compared with available experimental result under similar flow conditions. The difference between the experimental data and the present computational result is less than ±14%. It is seen that there is a good agreement between numerical and experimental values. It can therefore conclude that the present CFD results are valid.

Sl. No.	Reference	Geometry	Parameter	m = 0.005 (kg/s)	m = 0.01 (kg/s)	m = 0.015 (kg/s)
1	K. VasudevaKaranth [8]	W shaped corrugated absorber plate	Nusselt number(N_u)	16.9	28.4	38.6
2	Present CFD analysis	W shaped corrugated absorber plate	Nusselt number(N_u)	19.7	32.6	42.5

Table 7: Comparison between present CFD analysis and previous experimental results

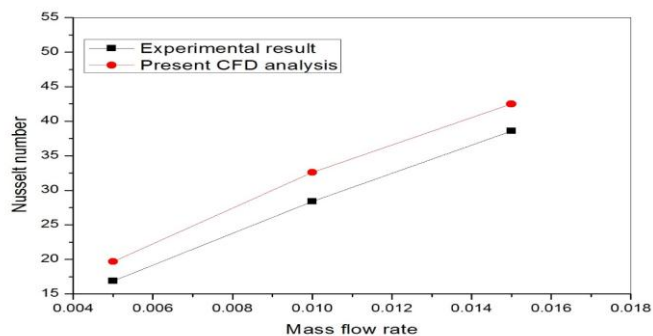


Figure 35: Variation of Nusselt number with mass flow rate for validation

V. CONCLUSIONS AND SCOPE FOR FUTURE WORK

On the basis of above investigation and results obtained following are the major conclusions have been made:-

- ✓ This review of literature reveals that a lot of work has been reported on design of solar air heater by experimental approach. This review also reveals that a few studies have been done on CFD analysis of solar air heater.
- ✓ A Computational Fluid Dynamics (CFD) analysis of solar air heater duct having corrugated absorber plate has been done. The results found from Dittus-Boelter and Blasius equation respectively is compared to Validate the turbulence model used for CFD analysis and it is found that Renormalization Group (RNG) k-epsilon turbulence model results show good agreement with the Dittus-Boelter and Blasius empirical correlation results.
- ✓ It is found that absorber plate with corrugated geometry helps to increase the Nusselt number of the air medium which in turn helps in enhanced convective heat transfer to the medium.
- ✓ The maximum thermo- hydraulic performance obtained from present work is 1.2357 at mass flow rate of 0.015kg/s.

FUTURE SCOPE OF THE PRESENT WORK

- ✓ The thermo – hydraulic performance can be find out for corrugated absorber plate for both experimental and computational way.
- ✓ Geometry of corrugation can be varied for analysis.

REFERENCES

- [1] J.L. Bhagoria, J.S. Saini, S.C. Solanki, “Heat transfer coefficient and friction factor correlations for rectangular solar air heater duct having transverse wedge shaped rib roughness on the absorber plate”, Renewable Energy, 25:341-69; 2002.
- [2] Karim A. and Hawlader M.N.A., “Performance investigation of flat plate, v-corrugated and finned air collectors”, Energy, 31:452-470; 2004.
- [3] Karim A., “Performance evaluation of a v-groove solar air collector for drying applications”, Applied Thermal Engineering, 26:121-130; 2006
- [4] Liu T. and Lin W., “A Comparative Study of the Thermal Performances of Cross-Corrugated and V-Groove Solar Air Collectors”, International Journal of Green Energy, 4: 427- 451; 2007
- [5] S.K. Saini, R.P. Saini, “Development of correlations for Nusselt number and friction factor for solar air heater with roughened duct having arc-shaped wire as artificial roughness”, Solar Energy, 82: 1118-1130; 2008
- [6] Vishavjeet S.H., Saini R.P., Saini J.S., “Performance of artificially roughened solar air heaters—A review”, J. Renewable and Sustainable Energy Reviews, 13:1854-1869; 2009

- [7] H. Benli, "Experimentally derived efficiency and exergy analysis of a new solar air heater having different surface shapes", *Renew. Energy* 50: 58-67; 2013
- [8] Karanth, Vasudeva K and Manjunath, M S and Sharma, Yagnesh N, "Three Dimensional CFD analysis of Solar Air Heater for Enhancement of Thermal Performance using Surface Corrugation". *International Journal of Earth Sciences and Engineering*, 6: 851-855; 2013
- [9] A.S. Yadav, J.L. Bhagoria, "Modeling and simulation of turbulent flow through a solar air heater having a square-sectioned transverse rib roughness on absorber plate". *Int J Heat Mass Transf*, 70:1024-1039; 2013.
- [10] Prasad B.N., "Thermal performance of artificially roughened solar air heaters", *Solar Energy*, 91: 59-67; 2013
- [11] Prasad B.N., Arun K., Behura, Prasad L., "Fluid flow and heat transfer analysis for heat transfer enhancement in three sided artificially roughened solar air heater", *Solar Energy*, 105: 27-35; 2014
- [12] Prasad BN, Kumar Ashwini, Singh KDP. Optimization of thermo hydraulic performance in three sides artificially roughened solar air heaters. *Sol. Energy*. 111; 313-319, 2015.
- [13] Behura AK, Prasad BN, Prasad L. Heat transfer, friction factor and thermal performance of three sides artificially roughened solar air heaters. *Sol. Energy*. 130; 46-59, 2016.
- [14] Kumar Ashwini, Prasad BN, Singh K D P. Thermal and thermo hydraulic performance of three sides artificially roughened solar air heaters. *IRJAES*, 2 (2), 215-231, 2017.
- [15] Behura, K. Arun, Rout, S. K., Pandya, H., Kumar, Ashwini. Thermal analysis of three sides artificially roughened solar air heaters. *Energy Procedia*. 109, 279-285, 2017.
- [16] Kumar Ashwini, Prasad BN, Singh K D P. Performance characteristics of three sides glass covered smooth solar air heaters. *Transylvanian Review*, 24 (11), 3247-3256, 2016.
- [17] Hwang JJ, Liou TM. "Heat transfer in a rectangular channel with perforated turbulence promoters using holographic interferometry measurement". *Int J Heat Mass Transfer*, 38:3197-3207; 1995
- [18] Buchlin J, "Convective heat transfer in a channel with perforated ribs". *Thermal Sci*, 41:332-340; 2002
- [19] Shaeri MR, Yaghoubi M. "International journal of heat and fluid flow numerical analysis of turbulent convection heat transfer from an array of perforated fins". *Int J Heat Fluid Flow*, 30:218-28; 2009
- [20] Kumar Ashwini. Plate temperature and heat transfer characteristics of three sides roughened and boosted solar air heaters. *IRJAES*, 1 (4), 168-172, 2016.
- [21] Kumar Ashwini. Thermal performance characteristics of three sides artificially roughened solar air heaters with and without booster mirrors. *IRJAES*, 1 (4), 161-167, 2016.
- [22] Kumar Ashwini, Alam Mahmood. A review on comparative study of thermal performance of artificially roughened solar air heaters. *IRJAES*, 1 (2), 4-12, 2016.
- [23] Kumar S, Saini RP. "CFD based performance analysis of a solar air heater duct provided with artificial roughness". *Renew Energy*, 34:1285-1291; 2009
- [24] Karmare SV, "Tikekar AN. Analysis of fluid flow and heat transfer in a rib grit roughened surface solar air heater using CFD". *Sol Energy*, 84:409-417; 2010
- [25] Boukadoum AB, Benzaoui A. "CFD based analysis of heat transfer enhancement in solar air heater provided with transverse rectangular ribs". *Energy Proc*, 50:761-772; 2014
- [26] Yadav AS, Bhagoria JL. "A CFD (computational fluid dynamics) based heat transfer and fluid flow analysis of a solar air heater provided with circular transverse wire rib roughness on the absorber plate". *Energy*, 55:1127-1142; 2013
- [27] Yadav AS, Bhagoria JL. "A CFD based thermo-hydraulic performance analysis of an artificially roughened solar air heater having equilateral triangular sectioned rib roughness on the absorber plate". *Int J Heat Mass Transf*, 70: 1016-1039; 2014
- [28] Yadav AS, Bhagoria JL. "A numerical investigation of square sectioned transverse rib roughened solar air heater". *Int J Therm Sci*, 79:111-131; 2014
- [29] Soi A, Singh R, Bhushan B. Effect of roughness element pitch on heat transfer and friction characteristics of artificially roughened solar air heater duct. *International Journal of Advanced Engineering Technology*, 1(3): 339-346; 2010
- [30] Giri AK. CFD analysis of reattachment point, heat transfer and fluid flow of a solar air heater duct provided with artificial roughness. M.Tech. dissertation. MANIT Bhopal, India; 2010.
- [31] Rajput RS. Heat transfer and fluid flow analysis of inverted U-type turbulator in a solar air heater duct by CFD. M.Tech. dissertation. MANIT Bhopal, India; 2010.
- [32] Sharma S, Singh R, Bhushan B. CFD based investigation on effect of roughness element pitch on performance of artificially roughened duct used in solar air heaters. *International Journal of Advanced Engineering Technology*, 2(1): 234-241; 2011
- [33] Sharma AK, Thakur NS. CFD based fluid flow and heat transfer analysis of a v- shaped roughened surface solar air heater. *International Journal of Advanced Engineering Technology*, 4(5):2115-2121; 2012
- [34] Gandhi BK, Singh KM. Experimental and numerical investigations on flow through wedge shape rib roughened duct. *The Institution of Engineers (India) Journal—MC* 90:13-18; 2010.